Non-linear MHD Simulations of Pellet Triggered ELMs in JET and ASDEX Upgrade tokamaks

S. Futatani[1,2], S. Pamela[3], G.T.A. Huijsmans[4], L. Garzotti[3], D. Frigione[5], A. Loarte[6], M. Hoelzl[7], P.T. Lang[7], G. Kocsis[8], F. Orain[7], M. Dunne[7], A. Lessig[7], M. Mantsinen[1,9], EUROfusion MST1 Team, ASDEX Upgrade Team, JET Contributors[10]

[1]*Barcelona Supercomputing Center (BSC-CNS), c/ Jordi Girona 29, 08034 Barcelona, Spain*
[2]*EUROfusion Consortium, JET, Culham Science Centre, Abingdon, OX14 3DB, UK*
[3]*EURATOM/CCFE, Fusion Association, Culham Science Centre, Abingdon, Oxon OX14 3DB, UK*
[4]*CEA, IRFM, F-13108, St-Paul-Lez-Durance, France*
[5]*Unità Tecnica Fusione, ENEA C.R. Frascati, via E. Fermi 45, 00044 Frascati (Roma), Italy*
[6]*ITER Organization, Route de Vinon sur Verdon, 13067 Saint Paul Lez Durance, France*
[7]*Max Planck Institute for Plasma Physics, Boltzmannstr. 2, 85748 Garching, Germany*
[8]*Wigner RCP RMI, Budapest, Hungary*
[9]*ICREA, Barcelona, Spain*
[10]*See the Appendix of F. Romanelli et al., Proceedings of the 25th IAEA Fusion Energy Conference 2014, Saint Petersburg, Russia*

Introduction

ITER operation in its high fusion performance DT scenarios relies on the achievement of the H-mode confinement regime, which is expected to lead to the quasi-periodic triggering of ELMs (Edge Localized Modes). The energy fluxes associated with natural ELMs will produce excessive erosion and/or superficial surface damage on the plasma facing components. Controlled triggering of ELMs by the injection of small pellets (small deuterium ice bodies) at frequencies significantly exceeding those of uncontrolled ELMs is one of the foreseen schemes to control ELM energy losses and divertor power fluxes in ITER. Although the technique has been demonstrated to decrease ELM size successfully in ASDEX Upgrade [1], JET [2], and DIII-D [3], uncertainties still remain regarding the physics understanding as well as of the consequence of its application, such as localised power loads associated with this technique [4]. Moreover, pellets may fail to trigger ELM for plasma scenarios in all metal wall ASDEX Upgrade which also requires better understanding of the underlying physical processes of the ELM triggering [8]
Modelling of ELM triggering by pellet injection for JET (#84690) and ASDEX Upgrade (#29178) discharges has been carried out with the non-linear MHD code JOREK [5, 6]. JOREK allows to determine the energy and particle losses by the pellet triggered ELM. Regarding the JET discharge simulation, the pellet is injected after the natural ELM simulation which allows to compare the power deposition profiles of natural and pellet triggered ELM.

Implemented pellet modelling in JOREK

The non-linear MHD code JOREK includes a model for the density source coming from the ablation of an injected deuterium pellet [5, 6]. The pellet is assumed to travel along a straight line with a given fixed velocity. The amplitude of the space and time varying density source is such that the integrated source rate is consistent with the NGS (Neutral Gas Shielding) pellet ablation model [7]. With non-linear MHD equations, the pellet ablation process is calculated self-consistently. The ablation of the pellet as it travels into the plasma causes a large local, moving density source. Since the deuterium pellet injection is mostly adiabatic,

the temperature at the location of the density source will drop such that the local pressure stays constant initially. Due to the large heat conductivity, the region over which the density perturbation extends will be quickly heated up. This results in a strong local increase of the pressure perturbation which triggers an ELM.

Modelling of pellet ELM triggering of ASDEX Upgrade plasma

The initial profiles for the modelling are extracted from the shot #29178 of the ASDEX Upgrade experiment. Plasma operation parameters are the plasma current of I_p = 1.0 MA, the toroidal magnetic field B_T = 2.5 T, NBI heating power P_{NBI} = 5.2 MW. Simulations have been carried out for pellet injection from the High Field Side (HFS) of the device [8]. The pellet size (initial pellet particle content) is varied in four steps such as $0.5x10^{20}$ D, $1.0x10^{20}$ D, $1.5x10^{20}$ D and $2.0x10^{20}$ D. The pellet ELM triggering dependence on the pellet size has been investigated keeping the injection velocity constant 240 m/s. JOREK simulations show that the pellet ablation leads to a growth of the MHD activity as reflected by the growth of kinetic and magnetic energy of the toroidal modes of n=1-10. For a small pellet size, smaller than $1.0x10^{20}$ D, the MHD activity decreases after the pellet is fully ablated and the pressure perturbation decreases as a consequence of the particle and energy transport processes. For large pellets, larger than $1.5x10^{20}$ D, a strong increase of the energy of the high toroidal modes, n>6 harmonics is observed in the simulations. The strong growth of the magnetic energy above a critical pellet size, corresponding to the growth of n=6-10 modes is interpreted as the ELM triggering by the pellet. Figure 1 shows the density contour of the poloidal plane during an ELM triggered by a large pellet ($2.0x10^{20}$ D). The ballooning mode structures which are directed to the core plasma are clearly observed in the HFS.

The JOREK modelling shows the time delay between the pellet arrival into the confined plasma and the ELM triggering is about 170 μs. Regarding the ELM size, the small pellet ($0.5x10^{20}$ D) causes losses of 0.38% of the total energy in 690 μs, and the large pellet ($2.0x10^{20}$ D) causes losses 2.4% of the total energy in 1240 μs. The time duration of the pellet triggered ELM obtained in the modelling is roughly consistent with the experiment result, where 10% of the plasma energy is lost in 3 ms with the injection of $1.5x10^{20}$ D pellet with 259 m/s [8].

The dependence of the power deposition asymmetry caused by pellet injection is also observed as shown in Fig. 2. This is consistent with the findings of DIII-D [6], and also with the modelling of JET plasma as shown in the next paragraph.

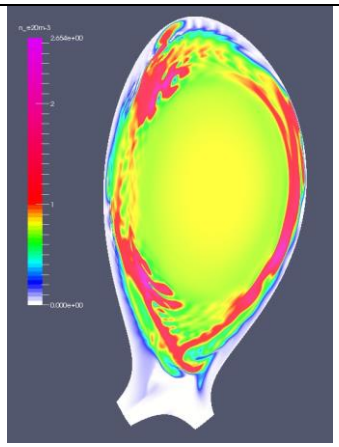

Figure 1. Contour plot of density during the pellet triggered ELM of the poloidal plane. The ballooning mode structures are clearly observed in the HFS.

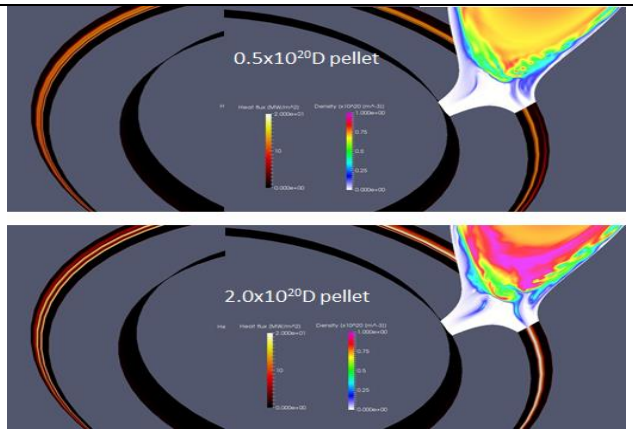

Figure 2. The profile of the heat flux on the outer divertor target by pellet injection of (top) small pellet and (bottom) large pellet. The toroidal asymmetry of the power deposition by pellet injection is observed.

Modelling of pellet ELM triggering of JET plasma

The initial profiles for the modelling are extracted from the shot of #84690 of the JET experiment. The plasma was a baseline H-mode scenario with toroidal magnetic field B_T = 2.1 T, plasma current I_p = 2.4 MA, and NBI heating power P_{NBI} = 10.5 MW. Simulations have been carried out for pellet injection from the outer midplane of the device which corresponds to the work of Ref [9]. Three pellet sizes have been studied; $0.5x10^{20}$ D , $2.0x10^{20}$ D and $3.5x10^{20}$ D. The pellet injection velocity is fixed to 78 m/s. Regarding the JET discharge simulation, the pellet is injected after the natural ELM simulation which allows to compare the power deposition profiles of natural and pellet triggered ELM.

The JOREK simulation has been launched without pellet injection, i.e. simulation of the natural ELM. When the natural ELM crash occurs, the profiles of the density and the pressure are relaxed because of the particle release. The simulation of natural ELM has been continued for a full ELM cycle, i.e. until the particle and energy loss stop, up to t=15415 μs. Thereafter, the pellet is injected. This approach corresponds to the pellet injection in the early phase of the ELM cycle, i.e. just after the previous ELM crash, therefore the plasma is far from the stability limit. The JOREK simulations show that the small pellet ($0.5x10^{20}$ D) does not trigger an ELM but the large pellet ($2.0x10^{20}$ D) triggers an ELM. The filamentary structures caused by the large pellet ($2.0x10^{20}$ D) injection are observed as shown in Fig.3. The width of the filamentary structures is not homogeneous as the pellet injection breaks the toroidal symmetry of the plasma. This is one of the characteristics of the pellet triggered ELM.

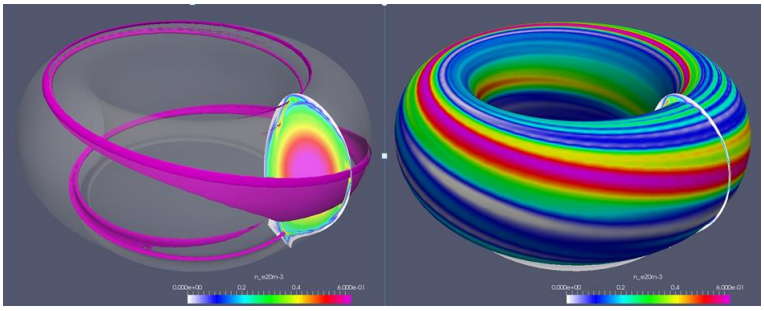

Figure 3. (left) The pellet cloud is shown in the pink band. The pellet from outer midplane ablates and the pellet cloud expands along the magnetic field line. (right) The density contour plot on the separatrix. The filamentary structures caused by the pellet are observed.

Regarding the ELM size of the natural ELM in the JOREK modelling, the plasma loses 12% of the total energy in 9 ms. The time delay between the pellet ablation onset and the ELM triggering is about 390 μs. Figure 5 shows the energy loss versus pellet size. The energy loss does not have a linear dependence on the pellet size. The small pellet ($0.5x10^{20}$ D) does not trigger an ELM, therefore, the energy loss is small. The large pellets (> $2.0x10^{20}$ D) trigger an ELM which leads large energy loss.

The difference comparison of the heat flux on the divertor tiles in the case of natural and pellet triggered ELM have been investigated. Figure 4 shows the heat flux on the divertor target during (top) the natural ELM and (bottom) the pellet triggered ELM. The profile of the heat flux caused by the natural ELM is toroidally symmetric. On the other hand, the pellet triggered ELM shows an asymmetric profile of the heat flux, i.e. a double peak on the right side. The second peak grows during the pellet triggered ELM. After the termination of the pellet ablation, the ELM behaviour relaxes and the second peak of the heat flux shrinks back. The appearance of the second peak is also observed in the JET experiment [4, 9].

Conclusion

The non-linear MHD simulations of pellet ELM triggering have been performed with JOREK code. The pellet size which is sufficient to trigger an ELM is estimated by the numerical modelling for ASDEX Upgrade and JET plasma. The power deposition asymmetry due to the pellet ELM triggering has been studied. The braking of the toroidal symmetry in the heat flux profile is observed, similar to the DIII-D study [6]. The JOREK modelling shows consistent observations with the experiment results.

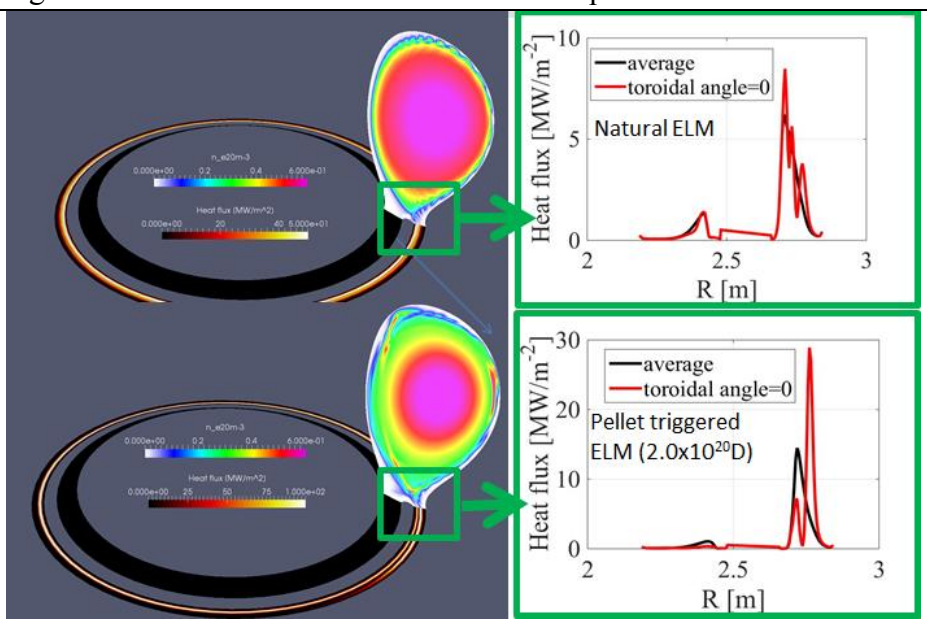

Figure 4. The heat flux on the divertor target during (top) the natural ELM and (bottom) the pellet triggered ELM. The profile of the heat flux caused by the natural ELM is toroidally symmetric. The pellet triggered ELM shows an asymmetric profile of the heat flux, i.e. a double peak on the right side. The appearance of the second peak is also observed in the JET experiment [9].

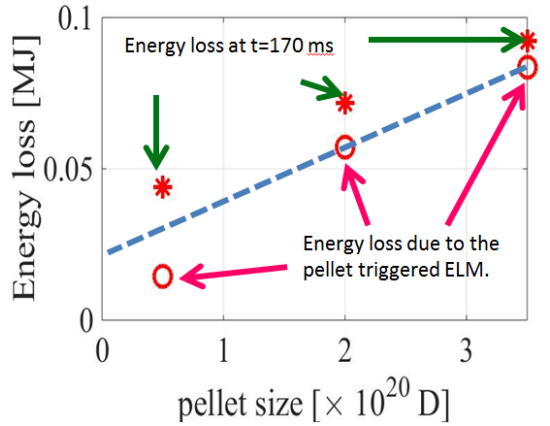

Figure 5. The energy loss versus pellet size. The dashed line is the scaling of the energy loss during the pellet triggered ELM.

Acknowledgements

This work has been carried out within the framework of the EUROfusion Consortium and has received funding from the Euratom research and training programme 2014-2018 under grant agreement No 633053. The part of the work was carried out using the HELIOS supercomputer system at Computational Situational Centre of International Fusion Energy Research Centre (IFERC-CSC), Aomori, Japan, under the Broader Approach collaboration between Euratom and Japan, implemented by Fusion for Energy and JAEA. We acknowledge PRACE for awarding us access to resource Mare Nostrum based in Spain at Barcelona. The author thankfully acknowledges the computer resources, technical expertise and assistance provided by the Red Española de Supercomputación. The views and opinions expressed herein do not necessarily reflect either those of the European Commission or those of the ITER Organization.

References

[1] P. Lang et al., Nucl. Fusion **44** 665 (2004). [2] P. Lang et al., Nucl. Fusion **53** (2013) 073010. [3] L. Baylor et al., Phys. Rev. Lett. **110** (2013) 245001. [4] R. Wenninger et al., Plasma Phys. Control. Fusion **53** (2011) 105002. [5] G.T.A. Huysmans and O. Czarny, Nucl. Fusion **47**, 659 (2007). [6] S. Futatani et al., Nucl. Fusion **54**, 073008 (2014). [7] K. Gal et al., Nucl. Fusion **48**, 085005 (2008). [8] P. Lang et al., Nucl. Fusion **54**,083009 (2014). [9] D. Frigione et al., J. Nucl. Materials **463**, 714 (2015).